JACS
JOURNAL OF THE AMERICAN CHEMICAL SOCIETY

Article

pubs.acs.org/JACS

Quantum Confinement-Tunable Ultrafast Charge Transfer at the PbS Quantum Dot and Phenyl-C_{61}-butyric Acid Methyl Ester Interface

Ala'a O. El-Ballouli,[†,§] Erkki Alarousu,[†,§] Marco Bernardi,[‡] Shawkat M. Aly,[†] Alec P. Lagrow,[†] Osman M. Bakr,[†] and Omar F. Mohammed*[,†]

[†]Solar and Photovoltaics Engineering Research Center, Division of Physical Sciences and Engineering, King Abdullah University of Science and Technology, Thuwal 23955-6900, Kingdom of Saudi Arabia

[‡]Department of Physics, University of California at Berkeley, Berkeley, California 94720-7300, United States

Supporting Information

ABSTRACT: Quantum dot (QD) solar cells have emerged as promising low-cost alternatives to existing photovoltaic technologies. Here, we investigate charge transfer and separation at PbS QDs and phenyl-C_{61}-butyric acid methyl ester (PCBM) interfaces using a combination of femtosecond broadband transient absorption (TA) spectroscopy and steady-state photoluminescence quenching measurements. We analyzed ultrafast electron injection and charge separation at PbS QD/PCBM interfaces for four different QD sizes and as a function of PCBM concentration. The results reveal that the energy band alignment, tuned by the quantum size effect, is the key element for efficient electron injection and charge separation processes. More specifically, the steady-state and time-resolved data demonstrate that only small-sized PbS QDs with a bandgap larger than 1 eV can transfer electrons to PCBM upon light absorption. We show that these trends result from the formation of a type-II interface band alignment, as a consequence of the size distribution of the QDs. Transient absorption data indicate that electron injection from photoexcited PbS QDs to PCBM occurs within our temporal resolution of 120 fs for QDs with bandgaps that achieve type-II alignment, while virtually all signals observed in smaller bandgap QD samples result from large bandgap outliers in the size distribution. Taken together, our results clearly demonstrate that charge transfer rates at QD interfaces can be tuned by several orders of magnitude by engineering the QD size distribution. The work presented here will advance both the design and the understanding of QD interfaces for solar energy conversion.

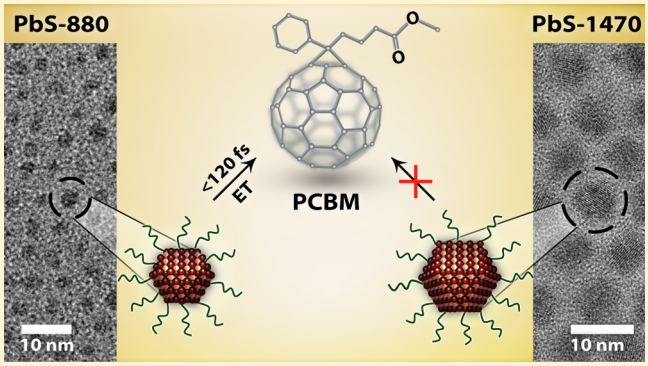

INTRODUCTION

Semiconductor quantum dots (QDs) have emerged as a new class of sunlight harvesting materials for photovoltaic (PV) solar energy conversion. QDs combine several advantages for use in PVs, including strong above-gap sunlight absorption, the possibility to tune the bandgap by controlling the QD size, solution processability, and the availability of a range of device architectures including p−n junctions and the depleted heterojunction.[1,2] In order to optimize QDs for PVs, it is crucial to understand the charge and energy transfer processes at QD interfaces. Specifically, efficient current generation in excitonic solar cells requires charge transfer (CT) at a donor−acceptor interface on a time scale much shorter than the lifetime of the excited state of the absorber.[3] This CT process is followed by charge separation to generate the electron and hole carriers that need to be collected at the electrodes before charge recombination.[3] Several reports have shown that increased bandgap energies in QDs (i.e., a smaller QD size) may promote,[4] suppress,[5] or rectify[6] electron transfer (ET) to other semiconductor nanostructures. In particular, recent work has focused on the importance of QD size in optimizing charge transfer and separation at QD/oxide interfaces,[4,6−8] thus enabling the use of QDs instead of dyes to realize quantum dot-sensitized solar cells (QDSSCs). Transient spectroscopic techniques have been recently employed to study ET from CdSe or CdS QDs to various acceptors including inorganic complexes,[9] organic compounds,[10,11] carbon allotropes,[12,13] and nanoparticles.[5,14,15]

However, CT kinetics in the most promising QDs for PV, namely, PbS QDs, remain largely unknown. Despite a few notable studies,[16,17] critical questions remain on how one can engineer efficient CT at interfaces based on PbS QDs by tailoring their size distribution. Tuning the size of QDs results in quantum confinement of the electronic states and constitutes a well-known strategy to regulate the electronic and optical properties of QDs. In particular, the bandgap and absorption spectrum of PbS QDs can be tuned by adjusting their size to harvest most of the incident solar spectrum. The ability to engineer fast and efficient ET in PbS QDs, or other QDs in

Received: December 31, 2013
Published: February 12, 2014

   dx.doi.org/10.1021/ja413254g | J. Am. Chem. Soc. 2014, 136, 6952−6959

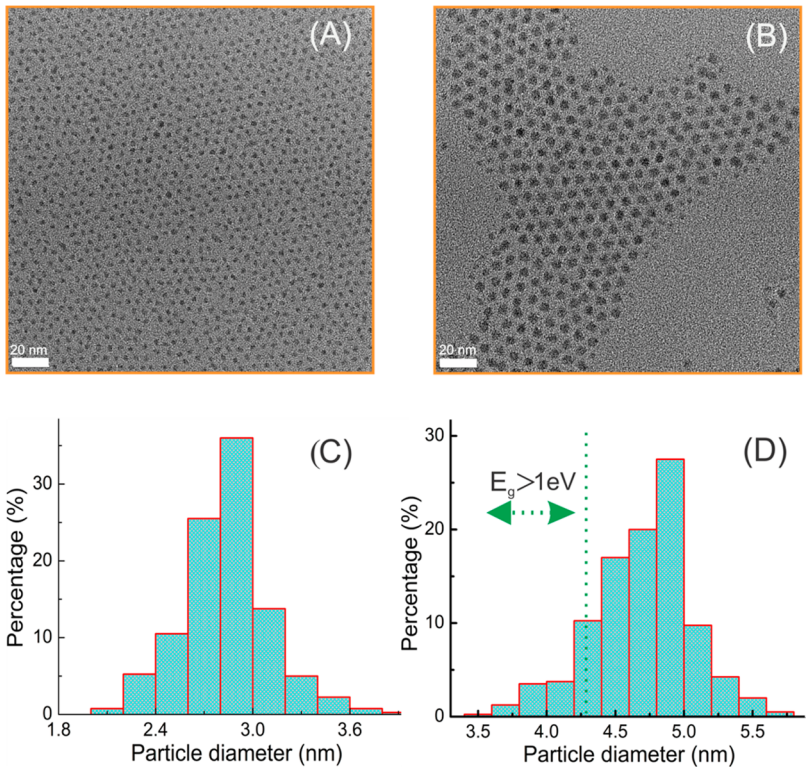

Figure 1. The top panel represents HRTEM of PbS-880 (A) and PbS-1320 (B) with 20 nm scale bars. The size distributions of PbS-880 (C) and PbS-1320 (D) were determined by measuring the diameter of 400 particles, and the average size of PbS QDs were found to be 2.84 ± 0.27 and 4.70 ± 0.36 nm, respectively. The size distribution of PbS-1320 shows the presence of some QDs with E_g > 1 eV.

general, may result in additional control of PV operation as well as efficiency enhancements. Quantitative data on ET dynamics can be directly resolved, with high precision, by applying broadband pump−probe spectroscopy to excite and detect the wavelengths around the first exciton absorption peak, typically located in the near-infrared region in PbS QDs. Using this approach,[18−20] one can directly investigate interface charge transfer, separation, and recombination in the time domain. The dynamics of such processes are crucial to understand the photophysical and photochemical processes in donor−acceptor systems.[21−24]

In this study, we combine femtosecond transient absorption (TA) spectroscopy with broadband capabilities and photoluminescence (PL) quenching measurements to investigate the effect of QD size variations on the dynamics of ET from PbS QDs to phenyl-C_{61}-butyric acid methyl ester (PCBM). PCBM was chosen as the electron acceptor for this study due to its wide use in PVs and its suitable electron affinity of 3.9 eV.[25] Our work analyzes the PL quenching signal in combination with the interface band alignment. We also decipher the signal for electron injection from photoexcited PbS QDs to PCBM, as inferred from the formation of the anionic species $PCBM^{\bullet-}$ with a temporal resolution of ∼120 fs. The TA results provide clear indication that the donor−acceptor interface alignment can be controlled by tuning the size distribution of PbS QDs. The charge transfer kinetics can be tuned from highly efficient and ultrafast (<120 fs) for PbS QD with a bandgap of more than 1 eV to nearly absent for PbS with larger diameters and a bandgap of less than 1 eV.

EXPERIMENTAL SECTION

Oleic-acid capped PbS quantum dots were synthesized using lead oleate and bis(trimethylsilyl)sulfide as precursors in 1-octadecene, as described by Hines et al.[26] (See the Supporting Information for details). The original colloidal solutions in toluene were washed twice with a methanol/toluene mixture and finally dissolved in octane. These stock solutions were diluted with 1,2-dichlorobenzene to an optical density (OD) of 0.1 at the first exciton absorption peak $1S_h \rightarrow 1S_e$ transition (i.e., equivalent to the lowest unoccupied molecular orbital−highest occupied molecular orbital (LUMO−HOMO) transition energy in organic molecules) in a 2 mm path length cuvette. Alternatively, the stock solutions were diluted with a certain concentration of PCBM in 1,2-dichlrobenzene, while maintaining an OD of 0.1 at the first exciton absorption peak. The steady-state absorption spectra of these solutions were measured using a Cary 5000 UV−vis−NIR spectrophotometer (Varian Inc.), while the steady-state photoluminescence spectra were measured using a Jobin−Yvon−Horiba Nanolog spectrofluorometer. Herein, we refer to the QD samples based on the wavelength of the $1S_h \rightarrow 1S_e$ transition; for example, the sample with the $1S_h \rightarrow 1S_e$ peak at 880 nm is named PbS-880.

Transmission electron microscopy was carried out on a TitanG2 80-300 instrument, FEI Co., Super Twin, x-FEG, operating at 300 kV. The PbS QDs suspended in octane solution were deposited onto 300 mesh gold grids with holey carbon film and dried in air for at least 1 h before imaging.

Time-resolved absorption decays were measured with a pump−probe setup where a white light continuum probe pulse was generated in a 2 mm thick sapphire plate contained in an Ultrafast System LLC spectrometer by a few microjoule pulse energy of the fundamental output of a Ti:sapphire femtosecond regenerative amplifier operating at 800 nm with 35 fs pulses and a repetition rate of 1 kHz. The spectrally tunable (240−2600 nm) femtosecond pulses generated in the optical parametric amplifier (Light Conversion LTD) and the white light continuum were used, respectively, as the pump

dx.doi.org/10.1021/ja413254g | J. Am. Chem. Soc. 2014, 136, 6952−6959

(excitation) and probe beams in the pump−probe experimental setup (Helios; see Supporting Information for details).

The PbS QD colloidal solutions (OD ≈ 0.1 at $1S_h-1S_e$ transition peak in 2 mm path length cuvette) were constantly stirred using a magnetic stirrer to provide a fresh sample for each laser shot and to avoid the photocharging of QDs.[27] The time-resolved experiments were performed at low pump fluence to ensure that the photoexcited QDs are due to single-photon absorption. This was done by maintaining the average number of photons (N_{ph}) absorbed per QD per pump pulse at the entrance face of our TA setup less than 0.2. Importantly, the absorption spectrum of each sample measured before and after every pump−probe experiment did not show any degradation.

RESULTS AND DISCUSSION

We employed different sizes of PbS QDs that absorb in the near-IR spectral region, ranging between 880 and 1470 nm. These QDs are nearly spherical in shape as indicated by the high-resolution TEM images in the top panel of Figure 1. The average size of the PbS QDs was calculated by measuring the diameter of 400 particles and was found to be 2.84 ± 0.27 and 4.70 ± 0.36 nm, for the small PbS-880 and large PbS-1320 QDs, respectively. These results are in very good agreement with the model proposed by Moreels, which relates the bandgap and diameter of PbS QDs:[28]

$$E_0 = 0.41 + \frac{1}{(0.0252d^2 + 0.283d)}$$

where E_0 and d are the bandgap and the diameter of PbS QDs, respectively. This model yields a predicted average size of 2.83 and 4.81 nm, for PbS-880 and PbS-1320, respectively.

Figure 2A,B show the changes in the steady-state absorption and PL spectra of PbS-880 and PbS-1320, respectively, upon the addition of different concentrations of PCBM, ([PCBM] = 0−50 mM). The well-defined absorption peaks (left panel) correspond to the $1S_h \rightarrow 1S_e$ transition, while the PL peaks (right panel) have a Gaussian shape with comparable full width at half-maximum (fwhm) indicating that the emission is due to a well-defined single quantum state. In the absence of PCBM, PbS-880 and PbS-1320 reveal PL emission at 992 and 1347 nm, respectively. Accordingly, the Stokes shift shows strong dependence on the QD size; while a 112 nm (0.159 eV) shift is observed for the small QDs, only a 27 nm (0.019 eV) shift is recorded for the large QDs. One proposed interpretation for the dependence of Stokes shift on the QD size is based on the presence of a gap state that moves together with the QD excitonic levels[29] and the observation of large Stokes shifts arising from a below-gap state that bears quantum confinement dependence and is largely modified by the QD size.[30] Another scenario addressed the phenomena by proposing the presence of a long-lived luminescent, size-dependent, in-gap state. In this case, radiative transitions can take place to the ground state either from higher (S_1) or lower (S_2) energy level;[31] the luminescence of small-size QD arises mainly from S_2, whereas the luminescence from S_1 is predominant in large QDs.[31]

The observed PL quenching of PbS QDs upon addition of PCBM indicates the presence of a photoinduced ET event between the PbS donor and the PCBM acceptor species.[1,32] While exciton quenching could also occur by energy transfer, here we rule out this mechanism due to the lack of spectral overlap between the absorption of PCBM and the emission of PbS QDs. A further consideration for donor−acceptor systems in the solution phase is whether fluorescence quenching is

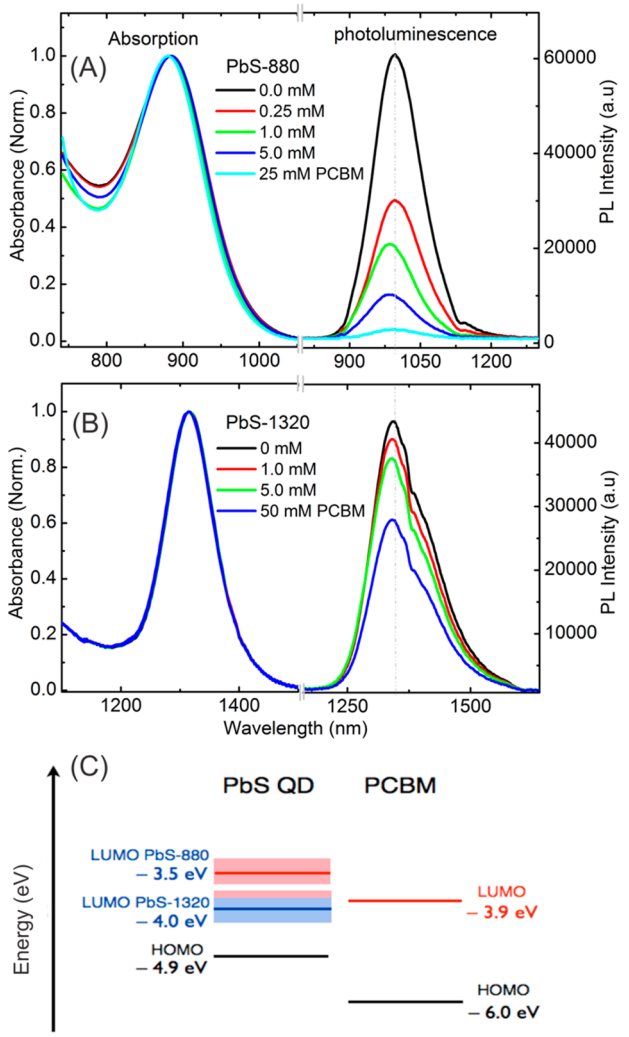

Figure 2. Steady-state absorption and PL spectra of PbS-880 (A) and PbS-1320 (B) upon the addition of different concentrations of PCBM in 1,2-dichlorobenzene. The PL spectra were recorded upon excitation with λ_{ex} = 890 nm and λ_{ex} = 1150 nm, respectively. The "dip" at 1380 nm in the PL spectra of PbS-1320 corresponds to an absoption peak of dichlorobenzene (see Supporting Information, Figure S3). (C) Interface band alignment between the two donors, PbS-880 and PbS-1320, and the PCBM acceptor. The HOMO and LUMO energies are shown. The HOMO and LUMO energies are provided as a range for the PbS donor to reflect the polydisperse size of the samples. The states contributing to CT from PbS-880 and the large-bandgap tail of PbS-1320 are shown in red in the PbS donor side, while the states not contributing to CT are shown in blue.

taking place via (1) static quenching whereby a nonluminescent ground-state complex is formed between the ground-state fluorophore and the quencher, (2) dynamic quenching, which involves the collision and subsequent formation of a transient complex between the excited-state fluorophore and the ground-state quencher,[33,34] or (3) a combination of both mechanisms. It was recently shown that the ET rate from QD to adsorbed electron acceptors increases with the number of acceptors;[10] hence, a stronger PL quenching is expected as the PCBM concentration increases. For PbS-880, the addition of 25 mM PCBM was sufficient to reduce PL emission to nearly null, Figure 2A, thus suggesting that the electron extraction by PCBM competes directly with electron−hole recombination processes. Also, the 25 mM PCBM addition resulted in a slight

dx.doi.org/10.1021/ja413254g | J. Am. Chem. Soc. 2014, 136, 6952−6959

blue shift of the PL peak (~15 nm, 0.019 eV) and the first exciton absorption peak (~4 nm, 0.0065 eV). This behavior may originate from the redistribution of electron density and is characteristic for the ground-state complex formation. The significant PL quenching observed here implies efficient electronic coupling between PCBM and PbS QDs in the ground state. Being in this regime, the spectral shift in the absorption and emission spectra, ultrafast electron injection to PCBM as inferred from the formation of the anionic species $PCBM^{\bullet-}$, and charge recombination as inferred from the ultrafast ground state bleach recovery (see below) provide clear indication for the ground state complexation and subsequent static electron transfer. These trends are in agreement with previous observations of electron transfer from PbS or CdS QDs to molecular acceptors.[35,36]

We have conducted quenching experiments to cover a large range of PCBM concentrations (0.01−25 mM) where a considerable PL quenching was observed. The constructed Stern−Volmer plot (see Supporting Information, Figure S2) shows the presence of two quenching regimes depending on the concentration of the quencher. At low PCBM concentration, the observed quenching can be assigned to a diffusion controlled mechanism. On the other hand, as the PCBM concentrations become relatively high, we observe a major contribution from the static quenching mechanism. This is indicated in the Stern−Volmer plot where a curvature was obtained when the relative emission intensity was plotted as a function of the quencher concentration (see Supporting Information, Figure S2). This curvature is understood in term of a saturation effect at the high concentrations of PCBM onto the PbS QD surface, leading to a complex formation that increases with the PCBM concentration, consistent with the static interaction.[37,38]

The substantial differences in the PL quenching behavior in PbS-880 vs PbS-1320 can be attributed to the band alignment between PbS dots of different diameters and the PCBM acceptor. Effective CT at the PbS/PCBM interface requires a type-II interface band alignment, as commonly found in other donor−acceptor systems.[39] Figure 2C shows the band alignment at the PbS/PCBM interface for PbS-880 and PbS-1320 QD samples. To derive the band alignment, we employed an ionization potential of 4.9 eV for PbS[40] and an electron affinity of 3.9 eV for PCBM.[25] Within this model, a PbS bandgap larger than ~1.0 eV is necessary to achieve type-II alignment, whereby the LUMO level of PbS is higher in energy than the LUMO level of PCBM, thus enabling effective electron injection from the excited state of PbS to PCBM. Since the exciton binding energy in PbS is small (~30 meV)[2] and comparable to kT at room temperature, excitonic effects do not alter charge injection based on a type-II electronic level alignment. We observe that the bandgaps of PbS-880 and PbS-1320 QDs with *ideally monodispersed diameters* are $E_g \approx 1.4$ eV and $E_g \approx 0.95$ eV, respectively, thus indicating that only the smaller PbS-880 dots can effectively inject electrons into PCBM. The PL quenching measurements for our PbS-880 and PbS-1320 solutions mixed with PCBM are consistent with this model, with slight deviations induced by the nonideally monodispersed size in our samples. In particular, since the critical gap of 1.0 eV corresponds to a 4.3 nm diameter, only QDs with $d < 4.3$ nm can contribute to charge transfer. The size distribution plots in Figure 1 show that all the QDs in the PbS-880 sample satisfy $d < 4.3$ nm and can thus contribute to charge transfer to PCBM, while in the PbS-1320 sample $d < 4.3$ nm holds only for a small-diameter tail of 13% ± 1% of the QDs (Figure 1D), as obtained by analyzing the diameter of over 400 QDs in a TEM microscope.

On this basis, we attribute the fast PL quenching observed in the PbS-880 to the presence of CT upon interaction of PbS to PCBM in solution, resulting in the quenching of the PL from the $1S_e \rightarrow 1S_h$ state of PbS. On the other hand, the near-absence of PL quenching in the PbS-1320 dots with smaller bandgap is consistent with the absence of type-II alignment and the presence of an energy barrier larger than kT for electron injection from photoexcited PbS to PCBM. We propose that the ~13% fraction of QDs with energy gap above ~1 eV are responsible for the residual CT and PL quenching in the PbS-1320 sample, leading to an overall slow rate for PL quenching as observed in our measurements. A quantitative analysis of the PL curves in Figure 2 supports this interpretation of the data. Table S1 (see Supporting Information) shows the peak PL intensity I_{PL} for 0, 1, and 5 mM concentrations of PCBM added to PbS-880 and PbS-1320 solutions, where the 0 mM sample corresponds to pristine PbS QDs.

The probability of residual PL events after addition of PCBM can be quantified by the ratio $R(c)$ of the PL intensity for concentration c of PCBM by the PL intensity in the absence of PBCM, $R(c) = I_{PL}(c)/I_{PL}(c=0)$. Within our model, we attribute PL quenching to charge transfer. Thus, for a PL quenching event to occur, PCBM and PbS with $d < 4.3$ nm need to encounter in solution, a process we associate with a probability $P_E(c)$, and then a CT event must occur following the encounter with a probability $P_{CT}(c)$. It follows that the probability for PL quenching at concentration c, $P_Q(c) = 1 - R(c)$, can be written as

$$P_Q(c) = P_E(c)P_{CT}(c) = 1 - I_{PL}(c)/I_{PL}(c = 0) \quad (1)$$

where the ratio in the righthand side of eq 1 can be computed using the data in Table S1, Supporting Information.

If our hypothesis that PL quenching is due to CT from PbS with $d < 4.3$ nm to PCBM is correct, comparison of the quenching probability P_Q for PbS-880 vs PbS-1320 for the same concentration c, and hence the same $P_E(c)$, should be related to the ratio of QDs with $d < 4.3$ nm in the two samples. In particular, since the fraction, f_{880}, of QDs in the PbS-880 sample with $d < 4.3$ nm is equal to unity ($f_{880} = 1$), while only a fraction of $f_{1320} = 0.13 \pm 0.01$ of QDs in the PbS-880 sample have $d < 4.3$ nm, we expect that for the same PCBM concentration, the following relation should hold:

$$\begin{aligned}(P_Q)_{880}/(P_Q)_{1320} &= (P_{CT})_{880}/(P_{CT})_{1320} \\ &\approx f_{880}/f_{1320} \\ &= 7.7 \pm 0.6 \end{aligned} \quad (2)$$

Using the I_{PL} data in Table S1, Supporting Information, we computed $(P_Q)_{880}/(P_Q)_{1320}$ values of 7.4 and 7.5, respectively, for $c = 1$ mM and $c = 5$ mM. These values are in excellent agreement with the range provided in eq 2 based on our assumptions of PL quenching events due to CT. This quantitative analysis constitutes a strong evidence that (1) PL quenching as observed in our experiments can be attributed to CT from PbS to PCBM and (2) CT to PCBM can occur only from PbS with $d < 4.3$ nm. We remark that while several authors have shown the tunability of the bandgap and photoabsorption in PbS QDs by controlling their size, our measurements highlight the important fact that by tuning the

dx.doi.org/10.1021/ja413254g | J. Am. Chem. Soc. 2014, 136, 6952−6959

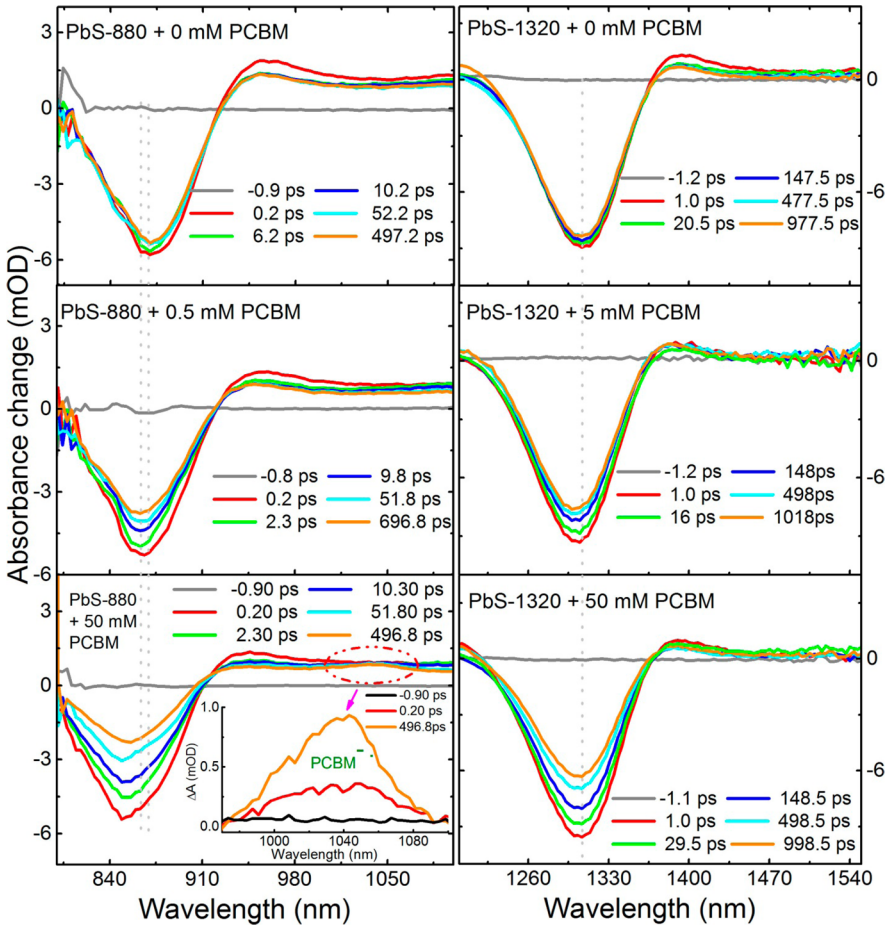

Figure 3. The averaged transient absorption (TA) spectra at indicated delay time windows following laser pulse excitation at $1.1E_g$ of PbS QDs, that is, 780 nm for PbS-880 (A) and 1200 nm for PbS-1320 (B), at increasing concentrations of PCBM.

diameter and bandgap of PbS, the interface band alignment can be changed from type-I (ineffective for CT) to type-II (effective for CT), similar to what has been found for interfaces of single-walled carbon nanotubes and PCBM.[41] Combined with the possibility to tune the size distribution of QDs during the synthesis, we conclude that PbS QDs constitute a platform with unique potential to control energy transfer (favored by type-I alignment) and charge transfer (favored by type-II alignment) at donor−acceptor interfaces.

Next, we studied the ground state bleach due to the $1S_h \rightarrow 1S_e$ transition in PbS QDs. Since this signal is directly associated with the electron population in the conduction band, we used it as a convenient probe to follow the carrier transfer and recombination dynamics. In particular, we used the ground-state bleach recovery to follow the charge recombination dynamics. The TA measurements of different PbS QDs sizes (PbS-1470, -1320, -1080, and -880) were recorded following laser pulse excitation at ∼1.1 times the bandgap, that is, 1340, 1200, 960, and 780 nm, respectively. It is worth pointing out that the optical excitation at $1.1E_g$ eV was chosen to avoid any contribution from the scattered light in the ground-state bleach signal, assuring high quality data and accurate dynamics for the ET process.

Figure 3 compares the TA spectra of the small (PbS-880) and large (PbS-1320) QD size in the absence and presence of different PCBM concentrations. The bandgap excitation of these QDs results in a bleaching maxima coinciding with the same wavelength of the first exciton absorption peak, referred to as the ground state bleach (GSB). In the absence of PCBM, the GSB reveals a very small decay in the picosecond time scale. This decay may be attributed to state trapping due to an incompletely passivated QD surface, and its amplitude was a few percent lower than the reported value for similarly sized PbS QDs.[42] This state trapping can provide additional recombination pathways.[43] As can be seen in Figure 3, the bleaching of the first excitonic peak (i.e., 1320 nm for large PbS and 880 nm for small PbS) was monitored upon increasing PCBM concentration. It is evident that higher PCBM concentration accelerates the GSB recovery (due to charge recombination) of PbS-880 much more than PbS-1320, providing clear indication of the formation of strongly coupled radical ions from effective ET from small diameter PbS QD to PCBM. Such an enhanced bleaching recovery further confirms the presence of an alternative deactivation pathway for charge carriers in smaller PbS, which implies effective electron injection from the conduction band of PbS to the LUMO of PCBM.[17] Moreover, the GSB feature of PbS-880 revealed a blue shift of a few nanometers upon the addition of PCBM, depending on the PCBM concentration, in perfect agreement with the shifts observed in the steady-state absorption measurements. Electron injection from PbS-880 to PCBM was monitored by the appearance of an absorption feature at a wavelength of ∼1040 nm, characteristic for a fullerene radical anion ($PCBM^{\bullet-}$),[44,45] providing conclusive experimental evidence for the ET event. As can be seen in Figure 3 inset, the electron injection to PCBM occurs within our temporal

dx.doi.org/10.1021/ja413254g | J. Am. Chem. Soc. 2014, 136, 6952−6959

resolution of 120 fs, which is orders of magnitude faster than the surprisingly slow ET time (~100 ns) measured between PbS and TiO_2,[46] thus confirming efficient electronic coupling between the conduction band of the PbS QDs and the LUMO of PCBM. Importantly, ET at a donor–acceptor interface is followed by ultrafast charge separation (CS) and recombination (CR). It is worth pointing out that the quantitative analysis for the CS dynamics is difficult to access for the following reasons: (i) both CR and CS occur on similar time scales, as the observed time evolution of the ion-pair population is a convolution of the two dynamics; (ii) PbS QDs show very strong and broad spectral feature due to the exciton absorption in the range of 900–1200 nm where the PCBM anion radical band is located (see Figure 3); in other words, the anion band is completely masked by the broad-spectral feature of PbS quantum dots; in addition, the PCBM anion radical band is extremely weak, which makes the quantitative analysis even more challenging, and (iii) more critically, the broad spectral feature (900–1200 nm) is dynamical in nature, which makes it very difficult, if not impossible, to do such analysis. This is why we presented the very early time (before decay) and very late time delay (after reaching plateau), as signatures for fast electron injection and charge separation processes, respectively.

Crucially, the $PCBM^{\bullet-}$ feature remained more pronounced for smaller QDs throughout our window frame (i.e., 500 ps), and GSB recovery reached a plateau (no further recovery), providing convincing evidence of the charge separation in which the radical ion pairs can be dissociated into free ions. This is supported by the energetic considerations, which is a convincing argument in favor of charge separation. Additionally, leveraging on the fact that the photocurrent generation requires CS, our observation of CS is supported by photocurrent measurements of PbS–PCBM blends where the photocurrent response was at least 2 orders of magnitude higher for the smaller PbS QDs compared with the larger ones.[17] Interestingly, the photocurrent in blends of PbS-1320 did not peak after excitation at the first exciton transition, but at shorter wavelength, a small photocurrent signal was measured and attributed to the smaller size distributions. These observations are fully consistent with our findings in terms of efficient ET and CS tuned by the quantum size effect.

Figure 4 shows a comparison of the GSB recovery dynamics on the picosecond time scale for different sizes of PbS QDs upon the addition of PCBM. The dynamics were fit to double-exponential functions with time constants of a few picoseconds and tens to hundreds of picoseconds that decrease as PCBM concentration increases as indicated in Figure 5. A global fitting procedure (see Supporting Information for details) for the bleach recovery of PbS-880, PbS-1080, and PbS-1320 indicated that not only is the percentage (%) recovery highest for the smaller PbS size, but also the rate of carrier recombination is affected by both the size of QDs and the PCBM concentration (see Figures 4 and 5). For instance, the recovery time constants, due to the carrier recombination, for PbS-880 are 23 and 513 ps at 0.5 mM PCBM and they shorten to 4.4 and 68.4 ps at 50 mM PCBM, indicating that the carrier recombination varies strongly with PCBM concentration. The observed two components point to the occurrence of two types of donor–acceptor ion pairs with different associated couplings. In other words, the GSB recovery of PbS-880 originates from donor–acceptor ion pairs with different distance or couplings, and these two kinds of ion pairs can be differentiated by their different recombination dynamics. The existence of different

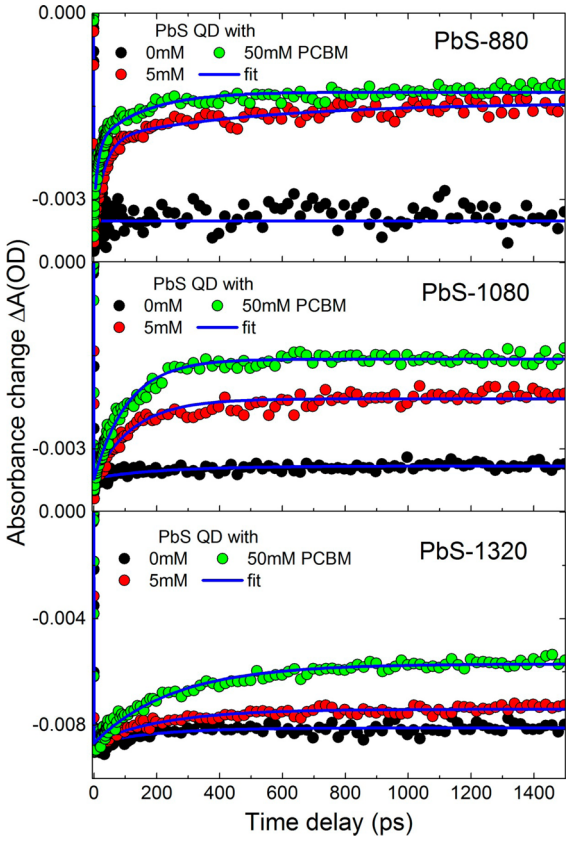

Figure 4. The time scales from the TA spectra of different sizes of PbS QDs (black traces) and solutions of PbS with 5 mM (red traces) and 50 mM (green traces) PCBM. The solid lines are fits of the kinetic traces. The plots clearly show a faster bleach recovery upon addition of PCBM to the smaller PbS QDs, followed by a slow component, while the kinetic traces of larger PbS QDs show only the slow component upon addition of PCBM.

types of ion pairs upon CT has been reported for other donor–acceptor systems.[47,48] Note that the low pump fluence (average number of photons absorbed per QD), less than 0.2, was used for all experiments. Hence, the probability of formation of multiexciton states through multiphoton absorption is negligible. PbS-1080 revealed similar behavior but with lower % recovery and significantly slower dynamics (see Figure 4). On the other hand, the kinetic behavior of PbS-1325 lacks the fast component and shows an overall lower recovery of ~30%, which is induced mainly by ~13% outliers in the size distribution. Finally, the recovery behavior of PbS-1470 with PCBM (see Supporting Information, Figure S4) lacks both fast and slow components, demonstrating that all the size populations for this sample are inactive for ET to PCBM. This evidence further verifies the size distribution and energy-level alignment analysis (as shown in Figure 2C) and supports strongly the fact that ET can be tuned by quantum confinement effects in the PbS QDs.

CONCLUSION

Efficient ET from QDs to TiO_2 is an essential process in Gratzel-type solar cells sensitized by semiconductor QDs. The rate of ET crucially competes with charge recombination during the PV operation, thus making it desirable to be able to tune the ET kinetics. Our results clearly demonstrate, for the first time, the possibility of modulating the ET rate between PbS

dx.doi.org/10.1021/ja413254g | J. Am. Chem. Soc. 2014, 136, 6952–6959

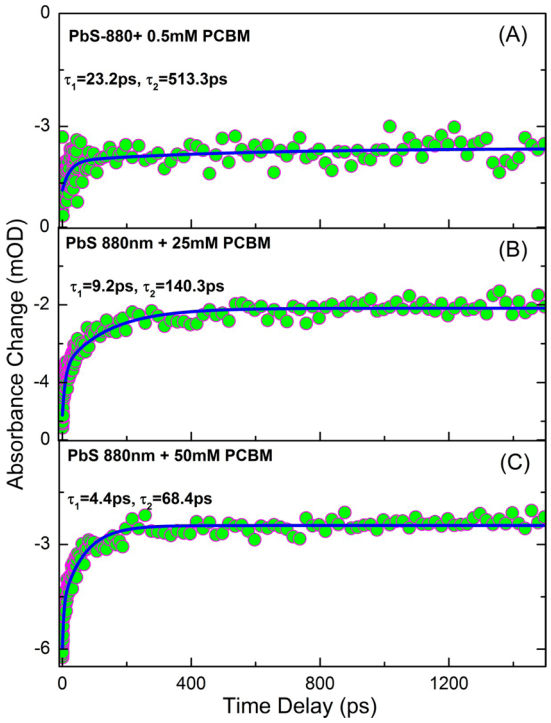

Figure 5. The time scales from the TA spectra of PbS-880 at different concentrations of PCBM. The dynamics were fit to double-exponential functions with time constants of a few picoseconds and tens to hundreds of picoseconds that decrease as PCBM concentration increases.

QDs and PCBM by tailoring the size distribution of PbS QDs due to quantum confinement effects. Our steady-state and time-resolved data demonstrate that only small-sized PbS QDs with a bandgap larger than 1 eV can inject electrons to PCBM upon optical excitation, as inferred from the formation of the anionic species $PCBM^{\bullet-}$. These trends are explained by the formation of a type-II interface band alignment controlled by the size distribution of the QDs via quantum confinement. In other words, the electron injection process can be tuned from highly efficient and ultrafast (<120 fs) for PbS QDs with a bandgap of more than 1 eV to nearly or completely absent for QDs with larger diameters and a bandgap of less than 1 eV. This information is of central importance to design of photovoltaic devices employing QDs to harvest the near-IR solar spectrum. Understanding the dynamics of the electron injection at the surface of the semiconducting QD is a key factor in determining the utility of these materials in applications that principally rely on the interfacial dynamics such as light-emitting diodes, p−n junctions, and photocatalysis.

■ ASSOCIATED CONTENT

Supporting Information

PbS QD synthesis details, PbS−PCBM solution preparation, experimental setup of TA spectroscopy, SV plot, emission "dip" explanation plot, and dynamics of PbS-1470. This material is available free of charge via the Internet at http://pubs.acs.org.

■ AUTHOR INFORMATION

Corresponding Author

omar.abdelsaboor@kaust.edu.sa

Author Contributions

[§]A.O.E.-B. and E.A. contributed equally to the work.

Notes

The authors declare no competing financial interest.

■ ACKNOWLEDGMENTS

Shawkat M. Aly is grateful for the post-doctoral fellowship provided by Saudi Basic Industries Corporation (SABIC). Cover design/illustration by Anastasia Khrenova.

■ REFERENCES

(1) Kamat, P. V. *J. Phys. Chem. C* **2008**, *112*, 18737.
(2) Sargent, E. H. *Nat. Photonics* **2012**, *6*, 133.
(3) Wrobel, D.; Graja, A. *Coord. Chem. Rev.* **2011**, *255*, 2555.
(4) Vogel, R.; Hoyer, P.; Weller, H. *J. Phys. Chem.* **1994**, *98*, 3183.
(5) Sant, P. A.; Kamat, P. V. *Phys. Chem. Chem. Phys.* **2002**, *4*, 198.
(6) Liu, D.; Kamat, P. V. *J. Phys. Chem.* **1993**, *97*, 10769.
(7) Zaban, A.; Micic, O. I.; Gregg, B. A.; Nozik, A. J. *Langmuir* **1998**, *14*, 3153.
(8) Kongkanand, A.; Tvrdy, K.; Takechi, K.; Kuno, M.; Kamat, P. V. *J. Am. Chem. Soc.* **2008**, *130*, 4007.
(9) Huang, J.; Stockwell, D.; Huang, Z.; Mohler, D. L.; Lian, T. *J. Am. Chem. Soc.* **2008**, *130*, 5632.
(10) Boulesbaa, A.; Issac, A.; Stockwell, D.; Huang, Z.; Huang, J.; Guo, J.; Lian, T. *J. Am. Chem. Soc.* **2007**, *129*, 15132.
(11) Sharma, S. N.; Pillai, Z. S.; Kamat, P. V. *J. Phys. Chem. B* **2003**, *107*, 10088.
(12) Robel, I.; Bunker, B. A.; Kamat, P. V. *Adv. Mater. (Weinheim, Ger.)* **2005**, *17*, 2458.
(13) Bang, J. H.; Kamat, P. V. *ACS Nano* **2011**, *5*, 9421.
(14) Chakrapani, V.; Tvrdy, K.; Kamat, P. V. *J. Am. Chem. Soc.* **2010**, *132*, 1228.
(15) Tvrdy, K.; Frantsuzov, P. A.; Kamat, P. V. *Proc. Natl. Acad. Sci. U. S. A.* **2011**, *108*, 29.
(16) Yang, Y.; Rodriguez-Cordoba, W.; Xiang, X.; Lian, T. *Nano Lett.* **2012**, *12*, 303.
(17) Gocalinska, A.; Saba, M.; Quochi, F.; Marceddu, M.; Szendrei, K.; Gao, J.; Loi, M. A.; Yarema, M.; Seyrkammer, R.; Heiss, W.; Mura, A.; Bongiovanni, G. *J. Phys. Chem. Lett.* **2010**, *1*, 1149.
(18) Cheng, P. Y.; Zhong, D.; Zewail, A. H. *J. Chem. Phys.* **1996**, *105*, 6216.
(19) Vauthey, E. *J. Photochem. Photobiol., A* **2006**, *179*, 1.
(20) Rosspeintner, A.; Angulo, G.; Vauthey, E. *J. Am. Chem. Soc.* **2014**, *136*, 2026.
(21) Nandwana, V.; Serrano, L. A.; Solntsev, K. M.; Ebenhoch, B.; Liu, Q.; Tonga, G. Y.; Samuel, I. D. W.; Cooke, G.; Rotello, V. M. *Langmuir* **2013**, *29*, 7534.
(22) Koch, M.; Rosspeintner, A.; Adamczyk, K.; Lang, B.; Dreyer, J.; Nibbering, E. T. J.; Vauthey, E. *J. Am. Chem. Soc.* **2013**, *135*, 9843.
(23) Nozik, A. J. *Inorg. Chem.* **2005**, *44*, 6893.
(24) Sykora, M.; Petruska, M. A.; Alstrum-Acevedo, J.; Bezel, I.; Meyer, T. J.; Klimov, V. I. *J. Am. Chem. Soc.* **2006**, *128*, 9984.
(25) Akaike, K.; Kanai, K.; Yoshida, H.; Tsutsumi, J. y.; Nishi, T.; Sato, N.; Ouchi, Y.; Seki, K. *J. Appl. Phys.* **2008**, *104*, No. 023710.
(26) Hines, M. A.; Scholes, G. D. *Adv. Mater. (Weinheim, Ger.)* **2003**, *15*, 1844.
(27) Hardman, S. J. O.; Graham, D. M.; Stubbs, S. K.; Spencer, B. F.; Seddon, E. A.; Fung, H.-T.; Gardonio, S.; Sirotti, F.; Silly, M. G.; Akhtar, J.; O'Brien, P.; Binks, D. J.; Flavell, W. R. *Phys. Chem. Chem. Phys.* **2011**, *13*, 20275.
(28) Moreels, I.; Lambert, K.; Smeets, D.; De, M. D.; Nollet, T.; Martins, J. C.; Vanhaecke, F.; Vantomme, A.; Delerue, C.; Allan, G.; Hens, Z. *ACS Nano* **2009**, *3*, 3023.
(29) Lewis, J. E.; Wu, S.; Jiang, X. J. *Nanotechnology* **2010**, *21*, No. 455402.
(30) Zhang, J.; Jiang, X. *J. Phys. Chem. B* **2008**, *112*, 9557.

(31) Litvin, A. P.; Parfenov, P. S.; Ushakova, E. V.; Fedorov, A. V.; Artemyev, M. V.; Prudnikau, A. V.; Cherevkov, S. A.; Rukhlenko, I. D.; Baranov, A. V. *Proc. SPIE* **2012**, *8564*, No. 85641Z.
(32) Ginger, D. S.; Greenham, N. C. *Phys. Rev. B: Condens. Matter Mater. Phys.* **1999**, *59*, 10622.
(33) Pesce, A. J.; Rosen, C. G.; Pasby, T. *Fluorescence Spectroscopy: An Introduction for Biology and Medicine*; Marcel Dekker: New York, 1971.
(34) Lakowicz, J. R. *Principles of Fluorescence Spectroscopy*; Plenum Press: New York, 1983.
(35) Knowles, K. E.; Malicki, M.; Weiss, E. A. *J. Am. Chem. Soc.* **2012**, *134*, 12470.
(36) Morris-Cohen, A. J.; Frederick, M. T.; Cass, L. C.; Weiss, E. A. *J. Am. Chem. Soc.* **2011**, *133*, 10146.
(37) Dibbell, R. S.; Watson, D. F. *J. Phys. Chem. C* **2009**, *113*, 3139.
(38) Cyr, P. W.; Tzolov, M.; Hines, M. A.; Manners, I.; Sargent, E. H.; Scholes, G. D. *J. Mater. Chem.* **2003**, *13*, 2213.
(39) Scharber, M. C.; Muehlbacher, D.; Koppe, M.; Denk, P.; Waldauf, C.; Heeger, A. J.; Brabec, C. J. *Adv. Mater. (Weinheim, Ger.)* **2006**, *18*, 789.
(40) Altavilla, C.; Ciliberto, E. *Inorganic Nanoparticles: Synthesis, Applications, and Perspectives*; Taylor and Francis Group: Boca Raton, FL, 2011.
(41) Bernardi, M.; Lohrman, J.; Kumar, P. V.; Kirkeminde, A.; Ferralis, N.; Grossman, J. C.; Ren, S. *ACS Nano* **2012**, *6*, 8896.
(42) Yang, Y.; Rodriguez-Cordoba, W.; Lian, T. *J. Am. Chem. Soc.* **2011**, *133*, 9246.
(43) Fitzmorris, B. C.; Pu, Y.-C.; Cooper, J. K.; Lin, Y.-F.; Hsu, Y.-J.; Li, Y.; Zhang, J. Z. *ACS Appl. Mater. Interfaces* **2013**, *5*, 2893.
(44) Guldi, D. M.; Prato, M. *Acc. Chem. Res.* **2000**, *33*, 695.
(45) Liedtke, M.; Sperlich, A.; Kraus, H.; Deibel, C.; Dyakonov, V.; Filippone, S.; Delgado, J. L.; Martin, N.; Poluektov, O. G. *ECS Trans.* **2010**, *28*, 3.
(46) Hyun, B.-R.; Zhong, Y.-W.; Bartnik, A. C.; Sun, L.; Abruna, H. D.; Wise, F. W.; Goodreau, J. D.; Matthews, J. R.; Leslie, T. M.; Borrelli, N. F. *ACS Nano* **2008**, *2*, 2206.
(47) Mohammed, O. F.; Adamczyk, K.; Banerji, N.; Dreyer, J.; Lang, B.; Nibbering, E. T. J.; Vauthey, E. *Angew. Chem., Int. Ed.* **2008**, *47*, 9044.
(48) Mohammed, O. F.; Vauthey, E. *J. Phys. Chem. A* **2008**, *112*, 5804.